

Hemodynamic alterations measured with phase-contrast MRI in a giant cerebral aneurysm treated with a flow-diverting stent

Matthew Ethan MacDonald, PhD; Parviz Dolati, MD; Alim P. Mitha, MD, SM; Muneer Eesa, MD; John H. Wong, MD, MSc; and Richard Frayne, PhD

Many risk factors have been proposed in the development of the cerebral aneurysms. Hemodynamics including blood velocity, volume flow rate (VFR), and intravascular pressure are thought to be prognostic indicators of aneurysm development. We hypothesize that treatment of cerebral aneurysm using a flow-diverting stent will bring these hemodynamic parameters closer to those observed on the contralateral side. In the current study, a patient with a giant cerebral aneurysm was studied pre- and postoperatively using phase-contrast MRI (PC-MRI) to measure the hemodynamic changes resulting from the deployment of a flow-diverting stent. PC-MRI was used to calculate intravascular pressure, which was compared to more invasive endovascular catheter-derived measurements. After stent placement, the measured VFRs in vessels of the treated hemisphere approached those measured on the contralateral side, and flow symmetry changed from a laterality index of -0.153 to 0.116 in the middle cerebral artery. Pressure estimates derived from the PC-MRI velocity data had an average difference of 6.1% as compared to invasive catheter transducer measurements. PC-MRI can measure the hemodynamic parameters with the same accuracy as invasive methods pre- and postoperatively.

Introduction

The prevalence of cerebral aneurysm is about 2.3% in the adult population (1). The etiology is unclear, but origin and development are thought to be affected by intravascular hemodynamic factors (2-4). Most brain aneurysms develop at regions with the highest hemodynamic stress, such

as bifurcations of the cerebral blood vessels. Cerebral aneurysms are usually discovered incidentally with neuroimaging during a neurological examination for other reasons. The annual rate of rupture has been estimated to be about 1% to 2% in most studies. The morbidity and mortality of a ruptured aneurysm is high. Standard treatments include surgical clipping and a variety of endovascular techniques, including coiling with and without balloon or stent assistance (5, 6). Recently, flow-diverting stents (like the Pipeline™ Embolization Device [PED] stent) have improved the treatment of large aneurysms. Comprehensive study of hemodynamic parameters in cerebral aneurysms is nonetheless challenging due to the high variability of aneurysm formation and the resulting geometry. However, wall-shear stress (WSS) (4), blood velocity, volume flow rate (VFR), and intravascular pressure (7-9) have been proposed as factors affecting aneurysm growth. VFR is known to be altered near to and distal to the aneurysm (10).

Different imaging modes have been used to examine aneurysms, including computed tomography (CT) and CT angiography (CTA), digital subtraction angiography (DSA), and magnetic resonance (MRI) angiography (3, 5, 8-9, 11-

Citation: MacDonald ME, Dolati P, Mitha AP, Eesa M, Wong JH, Frayne R. Hemodynamic alterations measured with phase-contrast MRI in a giant cerebral aneurysm treated with a flow-diverting stent. *Radiology Case Reports*. (Online) 2015;10(2);1109

Copyright: © 2015 The Authors. This is an open-access article distributed under the terms of the Creative Commons Attribution-NonCommercial-NoDerivs 2.5 License, which permits reproduction and distribution, provided the original work is properly cited. Commercial use and derivative works are not permitted.

Drs. MacDonald and Mitha are in the Department of Biomedical Engineering at the Hotchkiss Brain Institute, University of Calgary, Calgary, Alberta, Canada, and at the Seaman Family Magnetic Resonance Research Centre, Foothills Medical Centre, Calgary. Drs. Dolati, Eesa, Wong, and Frayne are in the Department of Radiology and Clinical Neuroscience, Hotchkiss Brain Institute, University of Calgary, Calgary, and at the Seaman Family Magnetic Resonance Research Centre, Foothills Medical Centre. Contact Dr. Frayne at rfrayne@ucalgary.ca.

Competing Interests: The authors have declared that no competing interests exist.

DOI: 10.2484/rcr.v10i2.1109

12). Estimation of hemodynamic parameters has been derived using many of these imaging modalities (3, 4, 13-16); however, there remains still much to understand with respect to 1) the relationship between hemodynamics and disease progression and 2) planning and evaluation of interventions using advanced hemodynamic parameters. We expected that VFR would become more symmetric across the brain after treatment with a PED stent, and that collateral flow would be reduced. We also hypothesized that VFR and pressure distal to the aneurysm would increase after deployment of a flow-diverting stent. Showing such changes is exceedingly difficult due to the heterogeneity of the aneurysm formation. Here, we report a clinical case that illustrates how PC-MRI can accurately estimate the hemodynamic parameters of interest in the cerebral aneurysm, pre- and post-intervention. As a secondary outcome, we show that upon successful deployment of a flow-diverting stent, the VFR and pressure measurements near and distal to the aneurysm become similar to values observed on the contralateral side.

Case report

Patient history

A 63-year old female presented with a three-week history of headache without significant triggers, including trauma. She described a throbbing pain, focused behind the left eye and in the temporal region, rating the pain as an eight or nine on a scale of ten. No seizures or other neurological symptoms were reported. The subject was a nonsmoker and nondrinker and was not taking any medication. Other medical history was unremarkable. Her general physical and neurological exams were normal. The intervention (described below) was successful, and the patient described an improvement in her headaches after one week. Informed written consent was obtained before research imaging.

Imaging

The patient underwent CT and CTA examinations, DSA during intervention, and three MRI examinations (one before the intervention and two after stenting). The CT/CTA and first MRI were performed before the procedure. The second and third MRIs were performed two and four days after the intervention, respectively. During the interventional procedure, injection runs were collected before and after stent deployment, visualizing the passage of the iodinated contrast agent and providing 3D spin angiograms. The DSA biplanar images were acquired at a rate of 4Hz. An injection protocol of 10ml injection at 5ml/s was used for each run.

The first and third imaging examinations used a 3 T MR scanner (Discovery 750 MR; General Electric Healthcare). The protocol included 1) localizer and sensitivity calibration scans, 2) noncontrast-enhanced time-of-flight (TOF) angiographic images, 3) several low- and moderate-resolution PC image volumes, and 4) a 4D flow imaging

sequence centered on the aneurysm region. Our initial strategy was to globally interrogate the larger vessels (with typical flow velocities on the order of 80cm/s to 100cm/s) and then to interrogate the cerebral aneurysm (with expected flow velocities on the order of 10cm/s to 20cm/s). Retrospective gating was used to reconstruct 30 cardiac phases per cardiac cycle. Imaging volumes were positioned to ensure overlap so that they could easily be combined during subsequent postprocessing steps. The second MRI used a 1.5-T MR scanner (Optima 450W, General Electric Healthcare) and was performed as part of standard clinical care. This imaging protocol included 1) T2-weighted, fluid-attenuated inversion recovery (FLAIR) imaging, 2) diffusion-weighted imaging (DWI), 3) susceptibility-weighted angiography (SWAN; General Electric Healthcare), 4) noncontrast-agent-enhanced TOF imaging, and 5) gadolinium contrast-agent-enhanced TOF imaging.

Endovascular intervention

The patient received antiplatelet therapy for a week before the operation. The intervention was performed with biplanar angiography guidance and under general anesthesia. A right common femoral artery puncture was made to introduce and advance a 6 Fr shuttle catheter (Cook Medical, Bloomington, IN) over a 5 Fr VTK-selective catheter (Cook Medical). Both devices were advanced over a 0.038-inch wire (Terumo, Somerset, NJ) and parked at the distal cervical ICA. Frontal and lateral angiographic images were acquired. Pressure measurements were taken with a catheter transducer around the aneurysm, in the cavernous ICA, and in the supraclinoid ICA and M1 segment of the ipsilateral MCA. Using standard endovascular techniques, a 4mm × 20mm flow-diverting stent (Covidien, Hazelwood, MO) was successfully deployed in the left cavernous ICA segment, across the neck of the aneurysm, with the distal end lying just proximal to the posterior communicating artery (PCoM) bifurcation. The stent fully covered the neck of the aneurysm. The stent was expanded with a balloon catheter (Hyperform; Covidien, Hazelwood, MO) for maximal stent-wall apposition. Additional DSA imaging indicated that blood flow was restored to vessels distal to the stent with stagnant blood inside the aneurysm. After the stent was deployed, the catheter transducer was again used to measure the pressure at the cavernous ICA proximal to the deployed stent.

Analysis

VFRs measured before and after the intervention in vessels proximal and distal to the aneurysm (with diameters >1 mm; see Table 1) were compared to the those of contralateral vessels, and the laterality index $[(L-R)/(L+R)]$, where L and R are the left and right flows, respectively] was calculated between paired vessels. Pressure estimates obtained with a catheter transducer were compared to measurements derived from the 4D flow measurements. A paired *t*-test was used to assess the significance of pressure changes between transducer and PC-MRI.

Hemodynamic alterations after flow-diverting stent

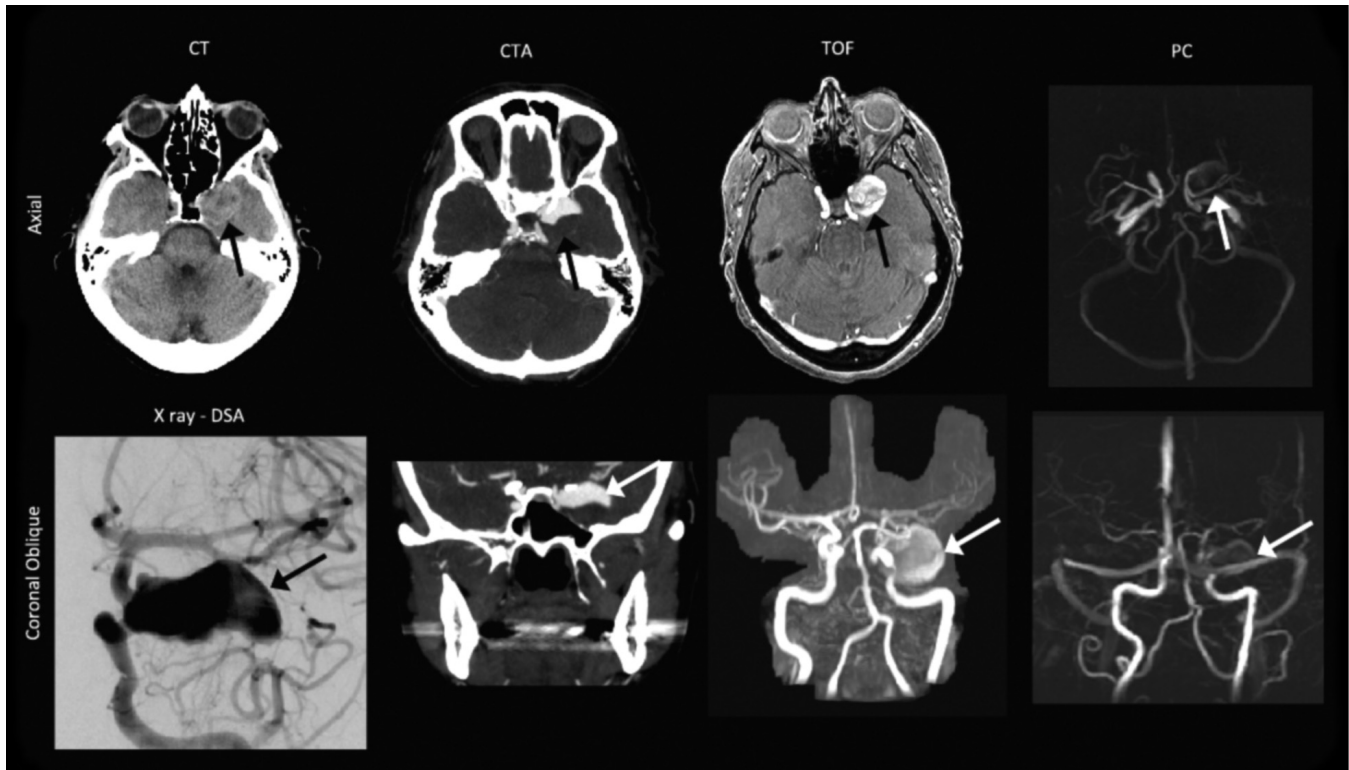


Fig. 1. Pre-operative computed tomography (CT), CT angiography (CTA), digital subtraction angiography (DSA), noncontrast-enhanced time-of-flight (TOF) imaging, and phase-contrast (PC) imaging. The aneurysm (black and white arrows) was clearly depicted on the combination of axial and coronal orientations. The coronal TOF and the PC images are maximum-intensity projections.

Imaging results

The CT scan revealed a large, unruptured, left cavernous internal carotid artery (ICA)-segment aneurysm (Fig. 1). The size of the aneurysm on noncontrast CT was 14mm x 23mm, with a 6mm-wide neck. The CTA showed filling of only the superior half of the fundus, suggesting that the inferior half of the aneurysm was filled with thrombus. The region that was filled with flowing arterial blood measured 14mm by 23mm. No ICA stenosis was found on imaging. MRI revealed that the aneurysm contained thrombus, filling the inferior portion. The TOF images clearly depicted the entire aneurysm, including the thrombus region (due to a shorter T1 relaxation time).

The PC images highlighted only the region of flowing blood. The high-resolution PC MRI-derived velocity measurements confirmed that the velocities toward the periphery of the aneurysm were on the order of 5cm/s, whereas samples in the center of the fundus were around 1.5cm/s (Fig. 2). Figure 2 also shows the force vectors generated by the blood. These vectors are analogous to the pressure, though they show the direction of the fluid force. A higher pressure was observed in the aneurysm where the flow jet reversed or where the velocity was small.

After the procedure (Fig. 3), the noncontrast-enhanced TOF angiography suggested no change in the size of the aneurysm. The region in the aneurysm previously filling

with blood was hypo-intense due to slower blood flow or partially coagulated blood. The contrast-enhanced TOF scan, like the DSA images, showed a small amount of contrast passing through the PED stent into the aneurysm. PC images showed that velocity in the treated aneurysm was <0.5cm/s. Blood velocity was observed to be higher in the arteries distal to the aneurysm, more closely matching velocity measurements from the contralateral side. As expected, MRI artifact (due to signal loss) was observed toward the outer edge of the vessel (that is, near the struts of the stent); however, the velocity at the center of the lumen and within the stent matched the proximal and distal velocity measurements. The additional clinical MRIs (FLAIR, DWI, and SWAN) did not demonstrate any changes in the brain due to stent deployment.

Volume flow rate results

The total blood flow entering the brain via the internal carotid and vertebral arteries was 6.8ml/s and 5.1ml/s pre- and postoperatively, respectively. Flow in the left ICA (where the stent was placed) increased as a percentage of total intracranial flow from 35% to 40% of total intracranial supply after the surgery (Table 1). The left MCA-M1 branches showed a VFR increase of 72% after stent deployment. The flow through the ACA arteries increased from 0.09ml/s to 0.11ml/s, due to flow being diverted past

Hemodynamic alterations after flow-diverting stent

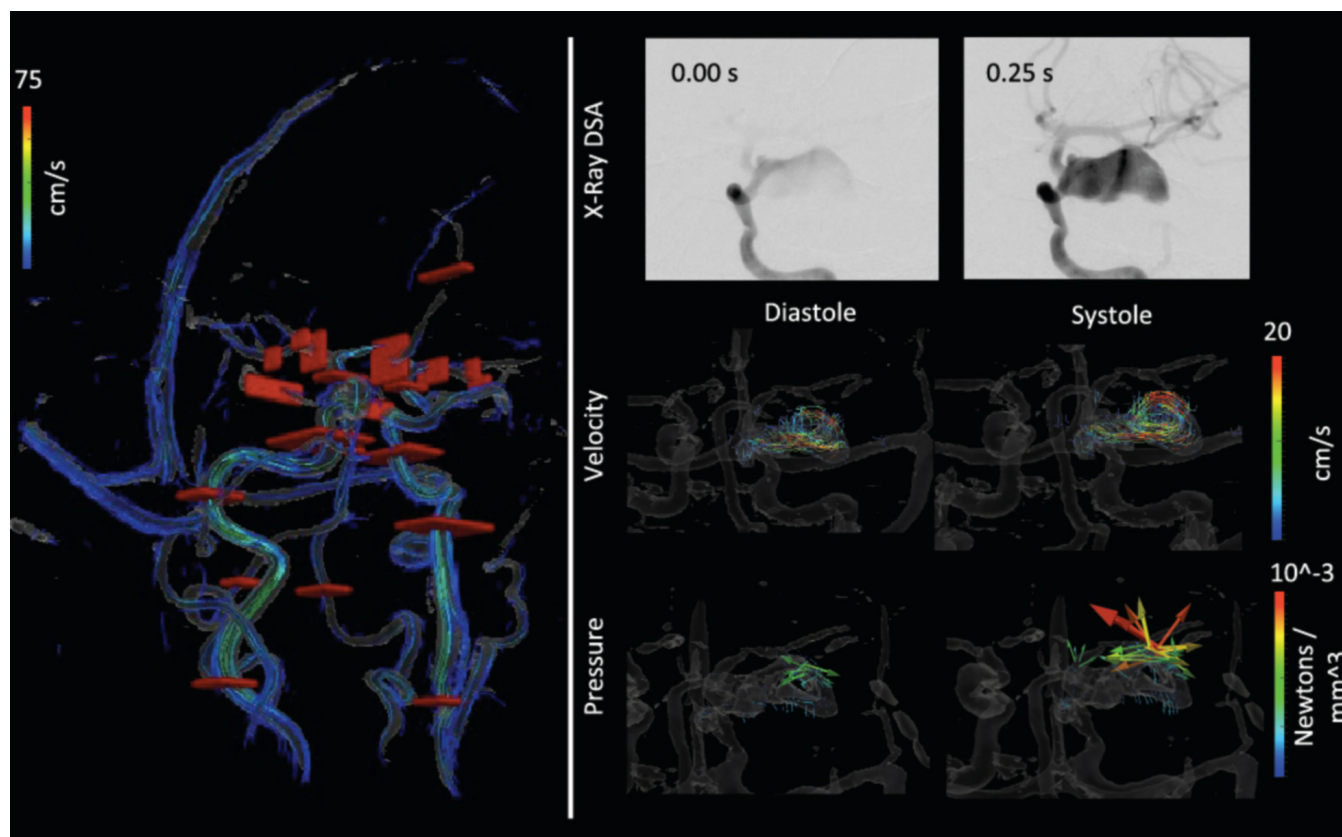


Figure 2: Cut planes used for flow volume calculations, temporal series of contrast inflow, and cine velocity and derived fluid force. Top: The cut planes (red surfaces) are shown over a rendering of the vascular structure and streamlines. Bottom: Upper row shows the contrast agent filling the fundus at 4 Hz; Middle row shows cine frames of the flow velocity; and Lower row shows the fluid force calculated from the Navier-Stokes equation at each pixel. Flow is observed to be higher toward the outer edge of the aneurysm, while forces are higher in the middle and toward the end, where the flow diverts backward.

the aneurysm because of the stent. Venous flow through the sinuses also showed a large postoperative change in the left-right VFR laterality index, similar to that observed in most intracranial arteries (Table 1).

Pressure measurement results

The pressure in the left cavernous ICA, measured with both the pressure transducer and the MR PC calculations, decreased postoperatively (Table 2). Conversely, pressure in the MCA M1 increased after the stent was deployed, concurrent with the increased blood flow observed in that vessel. A similar observation has been seen in pressure and VFR after aortic stenting (17). Catheter transducer pressure measurements could not be obtained postoperatively distal to the deployed stent (that is, supraclinoid ICA or MCA M1 segments) due to a risk of damaging the stent. MRI-derived pressure measurements could not be accurately measured inside the stent (near the supraclinoid ICA) due to image artifact. Overall, the PC-derived pressure measurements agreed with the catheter transducer measure-

ments. The average difference between the six matched pressure measures was 6.1%.

Discussion

Our study showed that PC-MRI can visualize and assess hemodynamic alterations after deployment of a flow-diverting PED stent. PC images were used to estimate velocity, VFR, and pressure both before and after the intervention. In this patient, the PED stent achieved its intended therapeutic effect of greatly decreasing flow into the aneurysm. The treatment also increased flow distal to the aneurysm and caused a flow reversal in the ACom arterial segment. Flow in the hemisphere contralateral to the aneurysm was reduced, resulting in the VFR in major arteries across the brain being more symmetric. PC data were also used to derive intravascular pressure, and the result was similar to the catheter transducer measurements.

Higher signal-to-noise TOF and PC images could be achieved by injecting a contrast agent (18-19) that decreased T1 relaxation times of blood. Noncontrast-agent-enhanced PC imaging was preferred in this study, as the

Hemodynamic alterations after flow-diverting stent

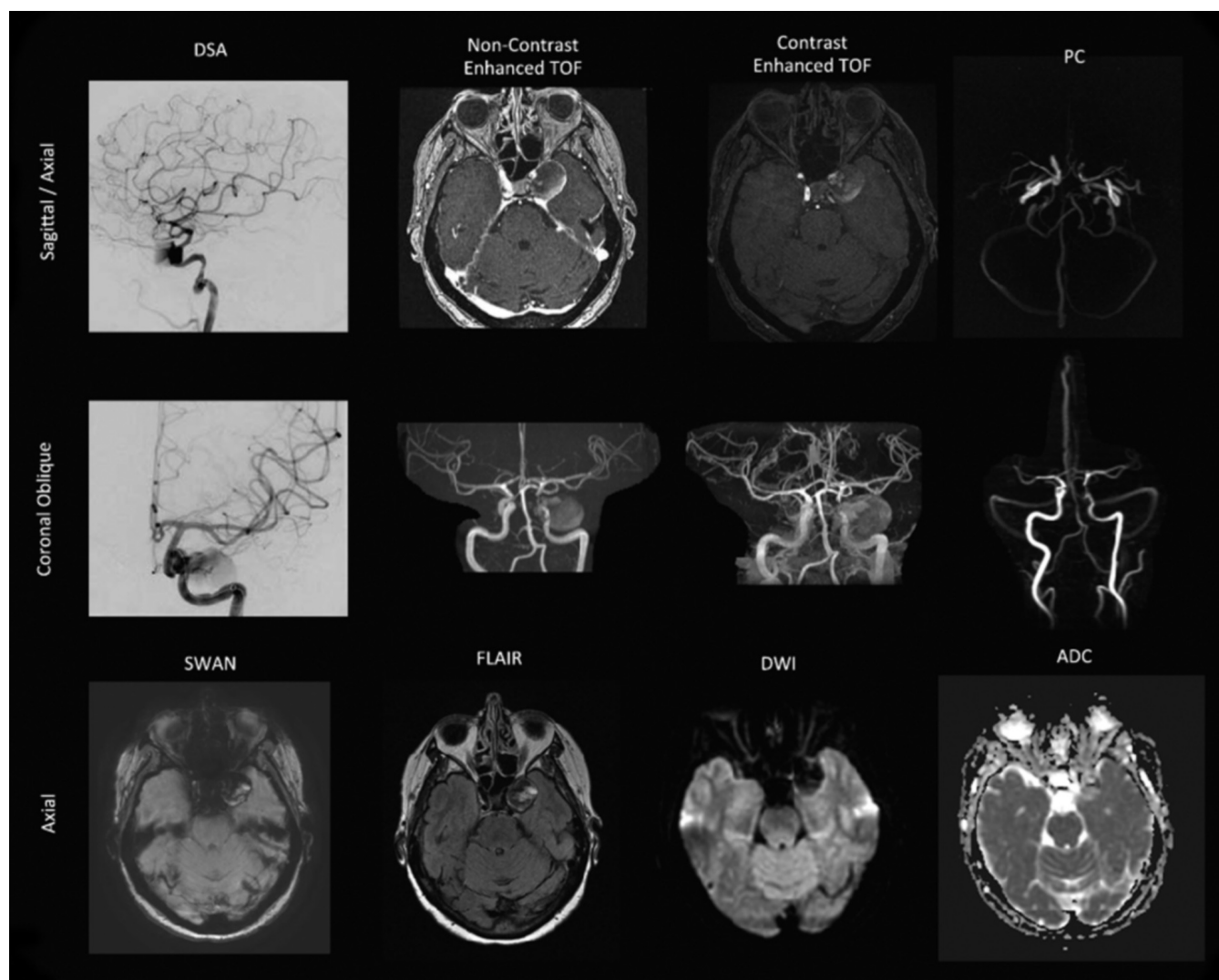


Figure 3: Postoperative imaging. DSA shows minor filling of the fundus as the contrast agent passes. This was supported by the MRI with noncontrast-enhanced and contrast-enhanced time-of-flight (TOF) and phase-contrast (PC) imaging. The aneurysm still appears large on TOF due to the short T1 of the thrombus. The phase-contrast images show near-zero velocity in the aneurysm. Susceptibility-weighted angiography (SWAN), T2-weighted fluid attenuated inversion recovery (FLAIR) imaging, diffusion-weighted imaging (DWI), and a calculated apparent diffusion coefficient (ADC) map transecting the aneurysm are also shown.

patient was already receiving several contrast-agent-enhanced scans with the clinical CTA, DSA, and MRI. MRI quality without contrast agent was sufficient for the analyses described here. The artifact from the stent, which was limited to a < 2mm region near the device, was consistent with previous studies and did not prevent estimation of flow in the middle of the parent artery (20). Small deviations in the pressure estimates could arise from a host of factors, including 1) the patient's being under general anesthesia, 2) the time of day and activity level, and 3) having catheters in the vessels during measurement. Other reports have focused on observing the pressure gradient along a

stenotic vessel in an animal model (9), providing quantitative measurements of flow.

Our objective in this case study was to thoroughly analyze the hemodynamic changes caused by the treatment. The current study demonstrates the ability to obtain pressure estimates with noninvasive PC-MRI in a clinical setting consistent with catheter transducer measurements. This was done through a battery of imaging techniques, each providing somewhat unusual information, while post-processing on PC-MRI images upheld our hypothesis that the flow would become more symmetric after treatment. Catheter transducer measurements and pressure derived

Hemodynamic alterations after flow-diverting stent

Blood vessel measured	Pre-operative		Postoperative		Relative change
	VFR (ml/s)	Laterality index	VFR (ml/s)	Laterality index	Absolute
Right Above Bifurcation ICA	3.05	-0.190	2.46	-0.095	-0.19
Left Above Bifurcation ICA	2.08		2.03		-0.02
Right Cervical ICA	3.37	-0.168	2.44	-0.048	-0.28
Left Cervical ICA	2.40		2.22		-0.07
Right Cavernous ICA	2.97	-0.350	1.98	---	-0.33
Left Cavernous ICA *	1.43		---		---
Right Supraclinoid ICA	1.25	-0.184	0.98	-0.116	-0.21
Left Supraclinoid ICA	0.86		0.78		-0.10
Right MCA M1	0.80	-0.153	0.47	0.116	-0.42
Left MCA M1	0.59		0.59		0.00
ACA	0.09		0.11		0.21
Acom †	-0.13		0.07		-1.52

Table 1. Volume flow rate (VFR) measurements in large anterior circulation vessels before and after stent deployment. Vessels were measured at the cut planes shown in Fig. 2. VFR is also normalized to the total flow entering the brain through the ICA.

ICA: Internal carotid artery. MCA: Middle cerebral artery. ACA: Anterior cerebral artery. Acom: Communicating artery.

* Indicates that measurements were not possible due to artifact from the stent.

† Negative sign indicates a flow reversal in the Acom, a change in the overall direction of the flow volume through the cut plane surface.

from PC-MRI both showed increased flow distal to the aneurysm.

This study showed how hemodynamic parameters are changed after flow diversion and that PC-MRI can measure the hemodynamic parameters with the same accuracy as invasive methods pre- and postoperatively. These techniques are a promising noninvasive method for assessment of pressure and flow alterations after deployment of a flow-diverting stent, and early detection of persistent hemodynamic stresses in a nonsecured brain aneurysm.

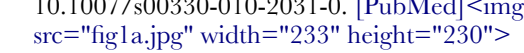
References

1. Rinkel GJE, Djibuti M, Algra A, van Gijn J. Prevalence and risk of rupture of intracranial aneurysms: A systematic review. *Stroke* 1998;29(1):251-6. [PubMed]
2. Cebral J, Putman C, Alley M, Hope T, Bammer R, Calamante F. Hemodynamics in normal cerebral arteries: qualitative comparison of 4D phase-contrast magnetic resonance and image-based computational fluid dynamics. *Journal of Engineering Mathematics* 2009;64(4):367-78. [PubMed]
3. Jou L-D, Lee DH, Mawad ME. Cross-flow at the anterior communicating artery and its implication in cerebral aneurysm formation. *J Biomech* 2010;43(11):2189-95. [PubMed]
4. Bousset L, Rayz V, Martin A, Acevedo-Bolton G, Lawton MT, Higashida R, et al. Phase-contrast magnetic resonance imaging measurements in intracranial aneurysms in vivo of flow patterns, velocity fields, and wall shear stress: Comparison with computational fluid dynamics. *Magn Reson Med* 2009;61(2):409-17. [PubMed]
5. Anxionnat R, Bracard S, Ducrocq X, Troussel Y, Lounay L, Kerrien E, et al. Intracranial aneurysms: Clinical value of 3D digital subtraction angiography in the therapeutic decision and endovascular treatment. *Radiology* 2001;218(3):799-808. [PubMed]
6. Claiborne Johnston S, Wilson CB, Halbach VV, Higashida RT, Dowd CF, McDermott MW, et al. Endovascular and surgical treatment of unruptured cerebral aneurysms: Comparison of risks. *Ann Neurol* 2000;48(1):11-9. doi: 10.1002/1531-8249(200007)48:1.
7. MacDonald ME, Dolati P, Mitha A, Wong JH, Frayne R. Phase Contrast Magnetic Resonance Imaging in Cerebrovascular Malformations: Towards Pressure Estimation. *International Magnetic Resonance Angiography Club*, 2013.

Hemodynamic alterations after flow-diverting stent

		Pressure measured		
Pre-operative		With catheter transducer	With PC-MRI	Percent difference
Cavernous ICA	Systolic	99mm Hg	99.6mm Hg	-0.6%
	Diastolic	62mm Hg	71.5mm Hg	-15.3%
Supraclinoid ICA	Systolic	85mm Hg	83.1mm Hg	2.2%
	Diastolic	55mm Hg	52.2mm Hg	5.1%
MC-M1	Systolic	76mm Hg	72.1mm Hg	5.1%
	Diastolic	52mm Hg	47.1mmHg	9.4%
Postoperative				
Cavernous ICA	Systolic	89mm Hg	84.2mm Hg	5.4%
	Diastolic	49mm Hg	51.7mm Hg	-5.5%
Supraclinoid ICA	Systolic	---		---
ACA	Diastolic	---		---
MC-M1	Systolic	---	82.1mm Hg	---
	Diastolic	---	54.6mm Hg	---

Table 2. Comparison of intravascular pressures using a catheter transducer versus PC-MRI. The average percent difference in measurements was 6.1%. Data is reported as systolic/diastolic pressure pairs.

8. Kecskemeti S, Johnson K, Wu Y, Mistretta C, Turski P, Wieben O. High resolution three-dimensional cine phase contrast MRI of small intracranial aneurysms using a stack of stars k-space trajectory. *J Magn Reson Imaging* 2012;35(3):518-27. [PubMed]
9. Moftakhar R, Aagaard-Kienitz B, Johnson K, Turski PA, Turk AS, Niemann DB, et al. Noninvasive Measurement of Intra-Aneurysmal Pressure and Flow Pattern Using Phase Contrast with Vastly Undersampled Isotropic Projection Imaging. *American Journal of Neuroradiology* 2007;28(9):1710-4. [PubMed]
10. Aenis M, Wakhloo AK, Lieber BB, Stancampiano AP. Modeling of Flow in a Straight Stented and Nonstented Side Wall Aneurysm Model. *J Biomech Eng* 1997;119(2):206-12. [PubMed]
11. Baert A, Knauth M, Sartor K. *Intracranial Vascular Malformations and Aneurysms*. Wanke I, editor: Springer; 2008.
12. Dempere-Marco L, Oubel E, Castro M, Putman C, Frangi A, Cebal J. CFD Analysis Incorporating the Influence of Wall Motion: Application to Intracranial Aneurysms. In: Larsen R, Nielsen M, Sporning J, editors. *Medical Image Computing and Computer-Assisted Intervention. Lecture Notes in Computer Science. 4191*: Springer Berlin Heidelberg; 2006. p. 438-45.
13. Schuster L, Schenk E, Giesel F, Hauser T, Gerigk L, Zabel-Du-Bois A, et al. Changes in AVM angio-architecture and hemodynamics after stereotactic radio-surgery assessed by dynamic MRA and phase contrast flow assessments. *Eur Radiol* 2011;21(6):1267-76. doi: 10.1007/s00330-010-2031-0. [PubMed] 
14. Frydrychowicz A, François CJ, Turski PA. Four-dimensional phase contrast magnetic resonance angiography: Potential clinical applications. *Eur J Radiol* 2011;80(1):24-35. [PubMed]
15. Valencia A, Morales H, Rivera R, Bravo E, Galvez M. Blood flow dynamics in patient-specific cerebral aneurysm models: The relationship between wall shear stress and aneurysm area index. *Med Eng Phys* 2008;30(3):329-40. [PubMed]
16. Alnæs MS, Isaksen J, Mardal K-A, Romner B, Morgan MK, Ingebrigtsen T. Computation of Hemodynamics in the Circle of Willis. *Stroke* 2007;38(9):2500-5. [PubMed]
17. Wendell DC, Samyn MM, Cava JR, Ellwein LM, Krolkowski MM, Gandy KL, et al. Including aortic valve morphology in computational fluid dynamics simulations: Initial findings and application to aortic coarctation. *Med Eng Phys* 2013;35(6):723-35. [PubMed]

Hemodynamic alterations after flow-diverting stent

18. Yang JJ, Hill MD, Morrish WF, Hudon ME, Barber PA, Demchuk AM, et al. Comparison of Pre- and Postcontrast 3D Time-of-Flight MR Angiography for the Evaluation of Distal Intracranial Branch Occlusions in Acute Ischemic Stroke. *American Journal of Neuroradiology* 2002;23(4):557-67. [PubMed]
19. MacDonald ME, Frayne R. Cerebrovascular MRI: a review of state-of-the-art approaches, methods and techniques. *NMR Biomed.* 2015;28(7):767-91. doi: 10.1002/nbm.3322.
20. Masaryk AM, Frayne R, Unal O, Krupinski E, Strother CM. In Vitro and In Vivo Comparison of Three MR Measurement Methods for Calculating Vascular Shear Stress in the Internal Carotid Artery. *American Journal of Neuroradiology* 1999;20(2):237-45. [PubMed]